

Preferential flow velocity mapping of alluvial soil using temporal electrical resistivity imaging

Todd Halihan¹  · Bharat S. Acharya¹ · John P. Hager¹ · Lucie Guertault² · Garey A. Fox²

Received: 3 November 2022 / Accepted: 28 December 2022

Published online: 10 January 2023

© The Author(s) 2023 [OPEN](#)

Abstract

Riparian soils are susceptible to the formation of macropores, which provide opportunities for preferential flow in comparison to the surrounding soil matrix. Temporal electrical resistivity imaging (TERI) can locate spatial heterogeneities in soil wetting patterns caused by preferential flow through macropores. Quantifying macropore flow properties is important to optimize the design of riparian buffers. In a field evaluation of a riparian area with naturally occurring macropores, the TERI technique is able to detect the wetted zone around a macropore similar to a high hydraulic conductivity zone in a heterogeneous soil matrix. An experiment was established in a coarse soil in North Carolina to evaluate if TERI datasets could quantify the hydraulic properties of both the soil matrix and the preferential macropore pathways. Results show TERI is a viable method for calculating the vertical fluid velocity along orthogonal profiles in this coarse-grained field site. The datasets allowed the distribution and hydraulic properties of the preferential flow pathways to be quantified over a two-dimensional plane that is comparable with traditional soil datasets.

Keywords Macropores · Preferential flow · Riparian soils · Hydraulic properties

1 Introduction

Preferential flow in soils can occur along any path of least resistance. The most common preferential flow pathway in soils are macropores, which are pores that vary in size and allow for rapid fluid migration in comparison to the surrounding matrix [1, 2]. Macropores account for only a small percentage of the total pore space in soils, yet they can dominate the flow and transport behavior, especially during heavy precipitation events [1, 3]. Preferential flow through macropores has been shown to occur under both partial water filling or drier surrounding matrix conditions [2]. Macropore flow can be a prevalent process promoting the transport of fertilizers and pesticides used in modern agricultural practices from fields to adjacent streams during precipitation events, resulting in impacts to surface water quality [4].

Riparian soils are susceptible to the formation of macropores, which have been shown to promote fast transport of water through soil layers. In such soils, preferential flow through soil macropores occurs due to enhanced biological activity, dry-wet cycles, and proximity to shallow water Tables [5, 6].

Research interest in macropore flow has largely shifted towards plot, field, hillslope, and catchment scale monitoring of macropore flow using geophysical imaging techniques and wireless moisture sensors in recent years [2, 7]. Geophysical tools like electrical resistivity imaging (ERI) could provide significant insight into the behavior of macropores

✉ Todd Halihan, todd.halihan@okstate.edu | ¹Boone Pickens School of Geology, Oklahoma State University, 105 Noble Research Center, Stillwater, OK 74078, USA. ²Biological and Agricultural Engineering, North Carolina State University, 102 Weaver Administration Campus, Campus Box 7625, Raleigh, NC 27695-7625, USA.



and preferential flow pathways in riparian soils. ERI techniques have been used by [4, 8–11], among others in studying macropore flow.

ERI is a noninvasive technique in which surface electrodes are used for collecting apparent resistivity data to infer hydrogeological properties and processes. The apparent resistivity data are inverted to obtain a modeled electrical resistivity (ER) image of the subsurface distribution of electrical properties ER is a function of soil moisture and fluid composition, as well as soil temperature, the distribution of soil particles and void spaces. ER values may vary from less than $1 \Omega \text{ m}$ for highly saline soil to $10^5 \Omega \text{ m}$ for dry soil overlying crystalline rocks [12, 13]. Dietrich et al. [8] demonstrated preferential flow of water using an ER technique and an infiltration test in a Paleudol soil with a petrocalcic horizon. More recently, ERI was used in identifying drying wetting patterns and determining the soil saturated hydraulic conductivity (K_s) following irrigation management [14].

Temporal Electrical Resistivity Imaging (TERI) consists of resistivity data acquisition from the same location at different time intervals. Differencing of ER images between time intervals can be used to delineate macropore structure and/or locate spatial heterogeneities in soil wetting patterns caused by preferential flow through macropores. These are important factors to consider to optimize the design and placement of riparian buffers [10]. In a field evaluation of a riparian area with naturally occurring macropores, the TERI technique could detect the wetted zone around a macropore similar to an area of increased hydraulic conductivity in a heterogeneous soil matrix. Halihan et al. [10] detected wetted zones around macropores using TERI under simulated rain and saturated infiltration tests in riparian soils. They also highlighted preferential flow through macropores can occur under unsaturated conditions. Quantifying macropore flow velocity remains a technically challenging task. Approaches to estimate macropore velocity include tracer travel time, macropore discharge, and rainfall-runoff lag time at soil cores to trench to field-profile scales [15].

The objective in this experiment is to attempt to detect and quantify macropore flow with saturated upper boundary conditions. In this study vertical soil moisture profiles were generated for three distinct scenarios depending on the surface boundary conditions: during rain/irrigation, a short time after rain/irrigation ended and long time after rain/irrigation ended. These soil moisture profiles provide a framework for interpreting the movement of water through the soil. The primary objective of this study was to evaluate preferential flow via mapping preferential flow velocity inferred with TERI profiles of alluvial soils. We hypothesized that TERI can be used to map fluid velocity in the subsurface because changes in electrical conductivity over time should show fluid migration through pulses of increased electrical conductance (decreased resistivity) generated from increased soil wetting. This coupled with the amount of time it takes for the pulses to wax and wane in a profile could delineate flow and allow macropore velocities to be quantified. Combining several TERI profiles in proximity will yield a map of the fluid velocity over an area where preferential flow can be identified by localized high flow velocity values.

The intent of this work is to use ERI and TERI monitoring to quantify the subsurface movement of water and to calculate the distribution of vertical preferential flow velocity values in the subsoil. This quantitative approach will contribute to precision agriculture and nutrient management in riparian zones and other environmentally sensitive areas, above some of the previously employed qualitative approaches. This work illustrates the importance of geoelectrical techniques to increase the data density across areas of interest by providing 2D and 3D views of infiltration processes. This work also provides an algorithm for velocity calculations, which can be employed in programming to automate TERI monitoring in hydrologic settings where infiltration is important, such as agriculture or managed aquifer recharge. This work is a step forward, paving the way for more refined hydrology models to precisely identify the hydrogeological characteristics of the subsurface using ERI and TERI monitoring.

2 Materials and methods

2.1 Site description

The field site was a 2-m wide \times 10-m long test plot located in Raleigh, North Carolina, USA ($35^\circ 45' 36.63'' \text{ N}$, $78^\circ 40' 44.23'' \text{ W}$) (Figs. 1 and 2). Raleigh has a humid-subtropical climate, with an average precipitation rate of 1170 mm/yr (46 in/yr) [16]. This site is characterized by a Pacolet sandy loam at the surface and Late Proterozoic-Cambrian lineated felsic mica gneiss beneath [17]. The survey area was situated over bare soil with vegetated woodland on the periphery. The plot was adjacent to a small, first-order stream which is a tributary of Lake Raleigh. The longest plot dimension was designed perpendicular to the contour of the soil in order to provide a downhill overland flow longitudinal to the plot (Figs. 1 and 2). Bedrock depth varies but was approximately 0.7 m from the surface. Upstream of the plot, the terrain was

Fig. 1 Diagram depicting the wetting domain in the NC site where wetting front velocity analyses were made. Line 1 is parallel with flow (blue arrow) while line 3 is perpendicular to flow crossing line 1 and the wetting domain. Lines 2 and 4 are greyed out due as they provided backup data for the primary datasets that was not required. Soil moisture data were collected in pits adjacent to the wetted area that are covered in blue tarps in Fig. 2a

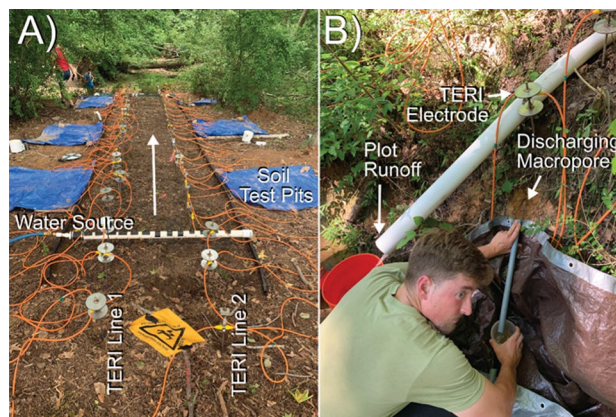
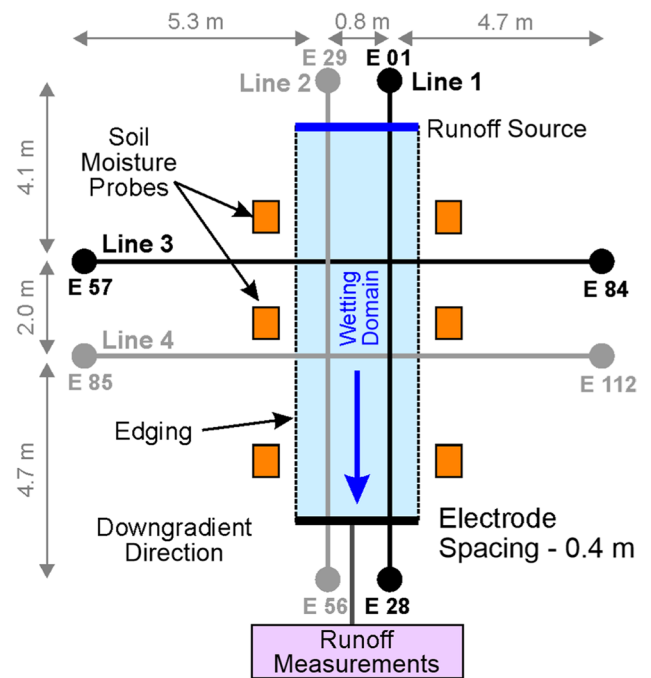


Fig. 2 Field photos of experimental setup. **A** Photo of the entire wetting domain in the North Carolina site. Line 1 is on the left, line 2 is on the right. Lines 3 and 4 are not set up in this photo. The wetting source is the black and white pipe in the foreground. Water flowed upward in the photo towards the break in slope at the end of the test area. Soil pits are covered in blue tarps. **B** Photo of coauthor John Hager at downgradient end of test plot showing white drain pipe with flowing plot runoff and active macropore flow draining from slope face into gray pipe

relatively flat, varying by a few cm in relief across the plot. The downstream end of the plot coincided with the edge of the streambank. Visible macropores were observed on the streambank at this edge of the plot.

2.2 Temporal electrical resistivity imaging and experimental setup

The test plot was bounded on the sides using landscape edging and consisted of four TERI lines, and six test pits with soil moisture probes. The plot was set up with a 0.8 m distance between TERI lines 1 and 2 and 2.0 m distance between TERI lines 3 and 4 (Figs. 1 and 2a). The runoff source was a 2-m wide perforated PVC pipe located 1.5 m down from the start of lines 1 and 2. It was used to simulate overland flow towards the stream. The soil moisture probes along each side of the wetting domain were part of the experiment conducted by Guertault et al. [18] and were installed in soil pits covered with blue tarps (Figs. 1 and 2a). Figure 2a shows just the wetting domain, with the view from the beginning with the wetting source in the foreground, looking down toward the end of the ERI lines within the wetting domain. The drop

in topography at the end of the image indicates the position of the downstream edge of the plot, coinciding with the streambank where flowing macropores were observed (Fig. 2b). A runoff collector was placed at this end of the plot to funnel overland flow to a short pipe used to measure runoff rates.

The test plot included four TERI lines, and an analysis of the data gathered to visualize what happened during the experiment. Briefly, the four TERI lines crossed perpendicularly to each other in duplicate pairs (Fig. 1). As the datasets for the experiment were composed of several images, and the cables were going to be left connected for the entire experiment. The duplicate lines were designed to manage potential data loss caused by equipment issues affecting one time interval or a cable eliminated by chewing from nocturnal animals. The intent was to use the orthogonal datasets with the most data and the lowest noise. Two of the lines were largely inside the experimental wetting domain and are referred to as the longitudinal lines. The other two lines only crossed through the domain and are referred to as the transverse lines. This wetting domain and specifically one TERI line of each orientation (TERI lines 1 & 3) were the primary focus for this section (Figs. 1 and 2). Line 1 was parallel with flow and exhibits the most change in topography. Line 3 was perpendicular to flow and crossed the wetting domain as well as line 1. This line was relatively flat with little changes in topography. Lines 2 and 4 collected data but were not included in the results as they were backups in the event of problems with Lines 1 and 3 (Fig. 1).

2.2.1 Wetting

In order to saturate the upper layer of the survey area, a 2-m wide water source was connected to a standard garden hose and dispersed water evenly over the width of the wetting domain via 1.5 cm diameter holes in a piece of PVC pipe (Figs. 1 and 2a). The water source was not moved during the experiment. The flow rate was 0.2 L/s (31.7 gpm) based on an average of discharge collections in a small 2-L bucket during 30 s intervals. The width of the plot was wetted from the source until the slope break and excess runoff was drained by a white PVC pipe (Fig. 2b).

2.2.2 TERI data collection

TERI datasets were collected with an Advanced Geosciences, Inc. (AGI) SuperSting R8 Resistivity Instrument. The instrument allows a user to collect and store apparent resistivity data. Multiple datasets can be processed to evaluate the changes in bulk resistivity that occurred between datasets to obtain TERI data. A relay switch box and four 28-electrode dumb cable were attached to stainless steel electrodes to survey the field site (Fig. 1). To power the instrument for data collection, a gas-powered generator and an AGI power supply box were used to convert the 110-V source from the generator to a 12-V source for the instrument. Once the survey lines were laid out in the field, the SuperSting field instrument measured apparent resistivity between electrodes and the data were processed and differenced using the Halihan/Fenstemaker algorithm [19, 20]. The algorithm excludes individual measurements with repetition error greater than 2%.

Five TERI datasets were collected for the experiment, two during soil wetting and three during drying. There were replicate samples longitudinal to flow and transverse to flow. The lowest noise datasets from each direction, TERI lines 1 and 3, were selected for analysis (Fig. 1). The times for imaging were selected based on previous experience in a gravel aquifer imaging experiment and previous experience with this site [20]. The imaging time for any image was less than an hour and previous experiments suggested that this did not lead to additional noise or that the flow processes would move faster than the imaging could capture [10, 20]. The first TERI dataset occurred after 30 min of wetting and the second at 2.5 h of wetting. Thereafter, the time elapsed was a drying time since the water source was discontinued. Datasets were collected at 2.0, 7.5, and 18.0 h after the wetting had ceased. Electrode spacing was 0.4 m, yielding a spatial resolution of 0.2 m in both longitudinal and transverse directions.

2.2.3 Soil data collection

Additional traditional soil data were available from moisture probes inserted in pits adjacent to the test plot at depths of 0.1, 0.2, 0.3 and 0.4 m (Figs. 1 and 2). These data were used as part of a separate study to determine the response of the soil and to model the macropore processes at the site [18]. The pits were excavated to the bedrock boundary.

Fig. 3 **A** Electrical resistivity profile for line 1 longitudinal to the flow of the runoff source prior to wetting. **B** Electrical resistivity profile for line 3 transverse to the flow of the runoff plot. Orange outlining indicates the sections where unsaturated flow was interpreted as migrating through the soil zone. Soil fluid velocity estimates were tabulated in Table 1

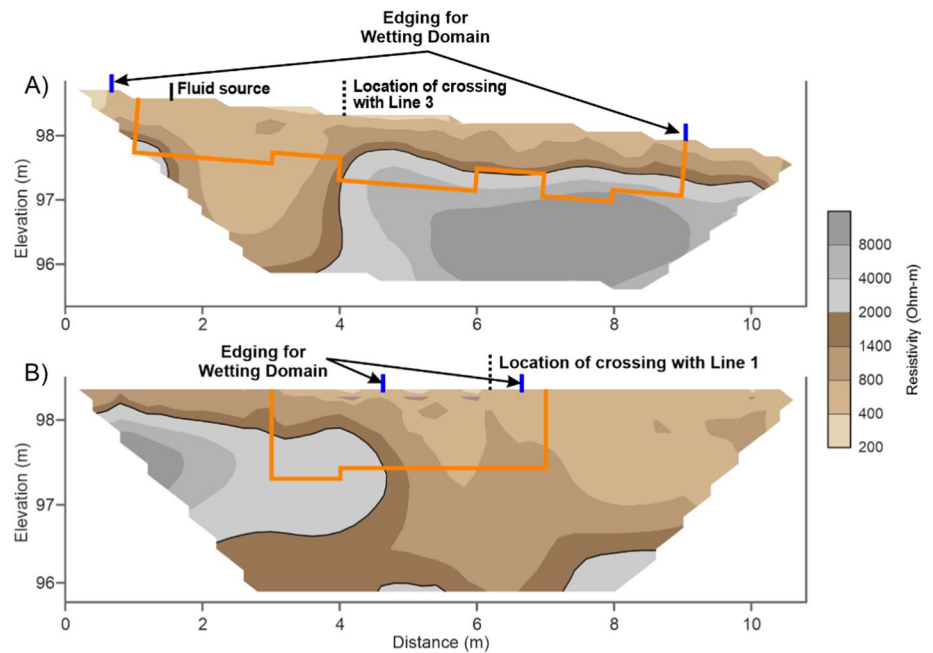
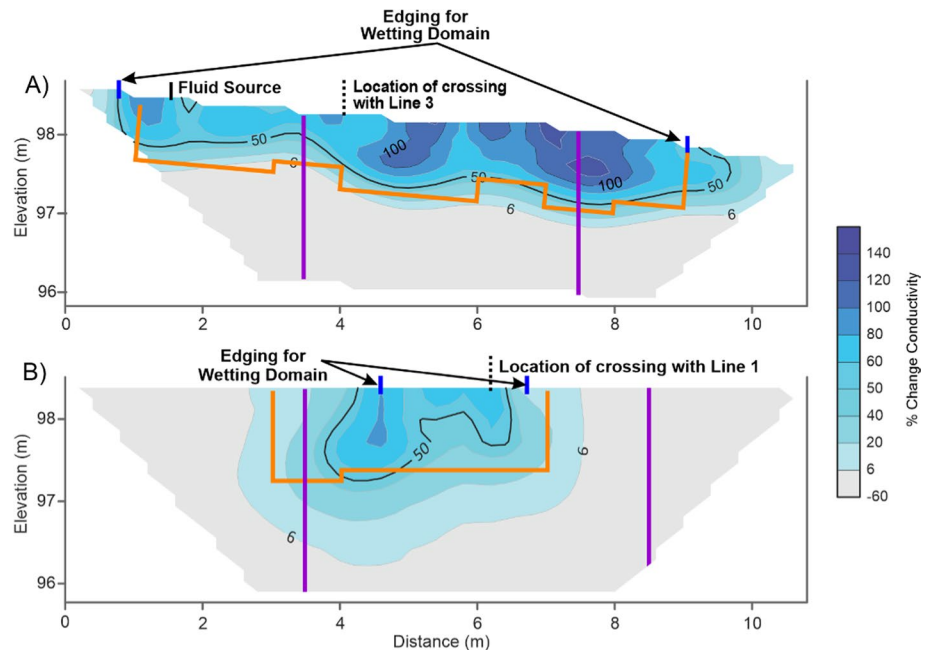


Fig. 4 **A** Change in Electrical conductivity profile of line 1 during wetting. **B** Change in electrical conductivity profile of line 3 during wetting. Orange outlining indicates the sections where soil fluid velocity was tabulated in Table 1 indicating the zones where fluids migrated through the vadose zone during the experiment. Vertical purple lines indicate the portions of the images that were used for analysis (Figs. 5, 6, 7, 8 and 9)



2.3 Data analysis

Once each ERI dataset was acquired from the field, they were inverted (Fig. 3) and differenced as a TERI dataset (Fig. 4) to determine the changes in electrical conductivity over time [20, 21]. The RMS error was evaluated for each single ERI inverted model resistivity dataset (3.5–7.2%) and each TERI differenced resistivity dataset (2.4–6.5%).

To measure vertical wetting along a single one-dimensional pathway, a single vertical line of TERI data was extracted from the datasets to evaluate vertical changes due to downward water flow in the profile. The TERI dataset consists of distance along the line, elevation, and a change in electrical conductivity. Analysis was performed using a single value for distance to obtain a dataset of elevation versus change in electrical conductivity. Vertical soil moisture profiles were created along TERI lines 1 and 3 every meter laterally from the left end starting at 1.5 m and ending at 8.5 m. Fluid velocities

were calculated from the vertical profiles (Figs. 5, 6, 7 and 8) by looking for the peak change in conductivity point and equating the depth of the peak change with the distance that the wetting front moved vertically into the soil over the duration of the experiment which is consistent with a previous TERI experiment for wetting front distance in macropores [10]. The vertical distance between peak conductivity change values on each curve against time from the last peak value provides as distance per time interpreted as a soil fluid velocity value. The peak values are labelled in time order for the

Fig. 5 Interpreted soil matrix flow observed at 3.5 m laterally along Line 1 (Fig. 4A). This is indicated through peak values on each curve moving down with moderate changes in conductivity. Green dots indicate peak resistivity values used for wetting front fluid velocity calculation. Vertical gray bar indicates noise estimate of 6%, and horizontal brown line is approximating soil-bedrock interface at 0.7 m depth below land surface

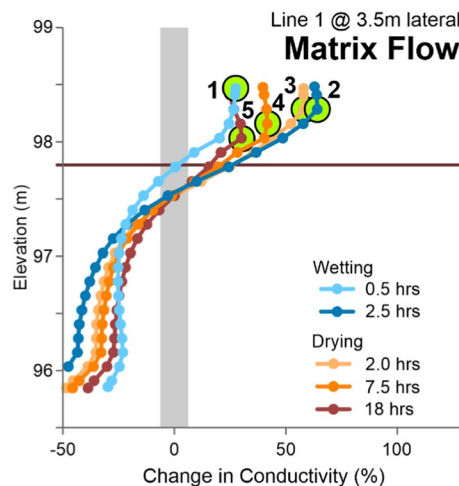


Fig. 6 Interpreted macropore flow observed at 7.5 m laterally along line 1 (Fig. 4A). Interpretation of macropore flow supported by depth of peak value reached with second curve (2.5 h) and staying consistent for each subsequent curve, as well as greater magnitude change in conductivity above 100% during the wetting period. Vertical gray bar indicates noise estimate of 6%, and horizontal brown line is approximate soil-bedrock interface at 0.7 m depth below land surface

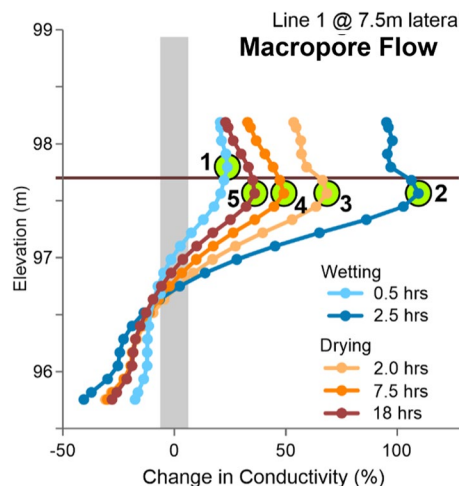
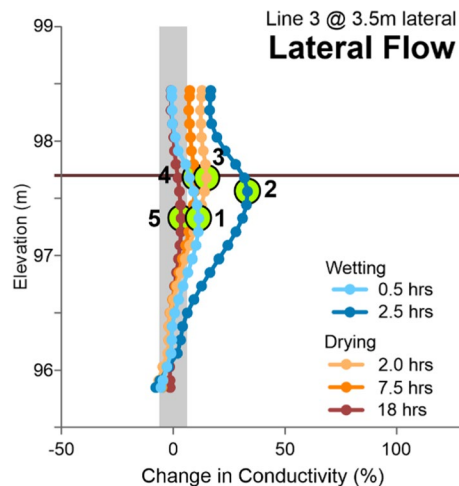


Fig. 7 Interpreted lateral flow observed at 3.5 m along transverse line 3 outside of the reaches from the wetting source (Fig. 4B). This location is 1.2 m away from the edge of the surface wetting domain. In this pattern, changes are smaller at the surface and larger at the soil-bedrock interface. Vertical gray bar indicates noise estimate of 6%, and horizontal brown line is approximate soil-bedrock interface at 0.7 m depth below land surface



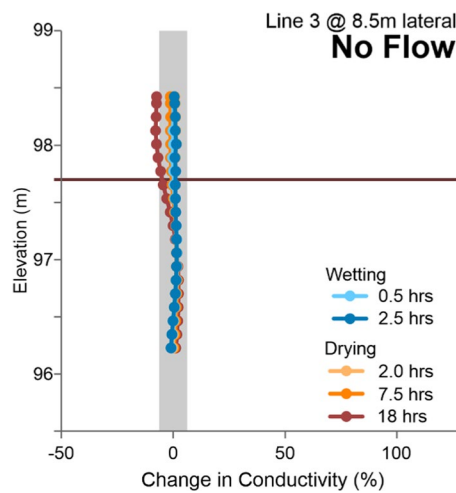


Fig. 8 No flow interpretation observed at 8.5 m laterally along transverse Line 3 (Fig. 4B). This location is 2.4 m away from the edge of the wetting domain where no moisture is expected to have changed during the experiment. The largest change in this pattern of the domain is a small negative change 18 h after wetting was discontinued which could be attributed to the surface soil drying during the day. Vertical gray bar indicates noise estimate of 6%, and horizontal brown line is approximate soil-bedrock interface at 0.7 m depth below land surface

five available TERI datasets (1–5) (Figs. 5, 6 and 7). Next, the vertical distance measured using TERI data peak grid nodes from the surface was used as the depth of the wetting front.

After evaluating the TERI data and extracting vertical change in conductivity data for each time period, every plot location per meter had vertical flow velocities calculated based on peak change in conductivity values for each time period. If no changes were detected between datasets, the vertical velocity was determined to be zero. This was common at the depth of the known soil-bedrock interface. Results were compiled to visualize the different velocities calculated laterally along the line (Table 1).

3 Results

3.1 Range and trends of resistivity values

The range and trends of resistivity were evaluated in the first imaging sequences of the experiment to determine background resistivity changes (Fig. 3). Static apparent resistivity images used as backgrounds for temporal analysis provide a range of resistivity values for the subsurface, denoting features such as lithological changes. Readings from 200 to 2000 ohm-m are colored in burgundy interpreted to correspond largely to the soil matrix. These values are relatively high resistivity for soil indicating a high porosity soil without significant amounts of electrically conductive clays [22]. Measurements greater than 2000 ohm-m are interpreted as low porosity bedrock, which is scaled in grey colors (Fig. 3).

3.2 Range and trends in temporal changes

Once the background was established, the range and trends of temporal changes were analyzed with subsequent imaging of the wetted plot compared to the background (Fig. 4). The TERI datasets had background noise levels of approximately 6% (Fig. 4) based on evaluating the data where no change should be occurring outside the wetting domain. TERI data above 6% change in bulk electrical conductivity was considered a signal indicating locations where soil moisture has changed. Changes in electrical conductivity between 6% and 50% were interpreted as areas typically dominated by soil matrix flow as they coincided with areas of slow vertical velocities. Areas that experienced a change in electrical conductivity greater than 100% were interpreted as flow domains typically dominated by preferential flow as they also generally reached the soil-bedrock interface; these areas also decreased in conductivity more rapidly during the drying phase. Areas with between 50% and 100% increase in bulk electrical conductivity were interpreted as a transition zone between matrix- and preferential flow- dominated areas.

3.3 Types of temporal changes

After each vertical profile had been processed, the types of temporal changes were evaluated. The four types of flow interpreted using TERI data were: matrix flow (Fig. 5), macropore flow (Fig. 6), lateral flow (Fig. 7), and no flow (Fig. 8). Longitudinal line 1 demonstrated both matrix (Fig. 5) and macropore flow (Fig. 6) profiles as each flow type was within the wetting domain (Fig. 4A). Transverse line 3 included both lateral flow profiles outside of the plot area (Fig. 7) and no flow regions (Fig. 8) as this perpendicular ERI line characterized results both inside and outside of the wetting domain. The resistivity changed the most during wetting with a peak value increasing in depth during the wetting phase. During the soil moisture redistribution phase with no surface water, the change in resistivity decreased over time and progressively deeper in depth for a simple soil wetting pattern which was located near the wetting source (Figs. 2 and 5).

Each interpreted flow pattern has distinctive characteristics for interpretation. Matrix flow (Fig. 5) showed a gradual increase of the depth at which the peak electrical conductivity was observed over time, labelled 1 through 5, indicating a sequential wetting pattern. During the wetting phase, the peak went from the surface to 18 cm depth with a peak change in conductance of 28% moving up to 64%. The drying values decreased gradually from 58 to 30% while slowly increasing in depth from 18 to 44 cm depth at the end of the experiment. As in a previous controlled macropore experiment [10], the TERI data shows a negative change in bulk electrical conductance below the wetted portion of the profiles (Figs. 5 and 6) which is an artifact of the data processing and gets a larger negative artifact at depth with the larger positive change in the soil profile. As the signals generated by the wetting should only be increases in conductance for much of the experiment, these deep artifacts were not interpreted as a signal in the experiments. A comparison of the patterns by focusing in on the positive changes above the soil-bedrock interface provides a more detailed view of the results (Fig. 9).

The interpreted macropore flow signature (Figs. 6 and 9b) exhibited an increase of the depth at which peak electrical conductivity occurred from times 1 to 2 (wetting phase), but during the drying phase (times 2 to 5), the peak electrical conductivity value remained at the same depth. During wetting, the change in conductance went from 32 to 127% at depths from 39 cm down to 63 cm, which is at or below the estimated soil-bedrock interface. During the drying phase, the change in conductance decreased from 81 to 46%, but the depth remained constant. This response was interpreted as rapid saturation where the wetting front reached the lithological boundary quickly. Matrix flow and preferential flow differed in the time elapsed to reach the same level of vertical saturation in the profiles with differing magnitude of change of electrical conductance. Preferential flow velocities were two to three orders of magnitude greater than matrix flow velocities.

The interpreted lateral flow pattern (Fig. 7) included changes in electrical conductivity significant enough to record peak values outside of the wetting domain. The peak values, however, were sporadic and do not follow a pattern similar to matrix and macropore flow. The values appeared at the soil-bedrock interface, and surface changes were not observed. Lastly, the no flow pattern (Fig. 8) had no peak values above background as this area was far enough from the wetting domain to remain dry during the entire experiment.

3.4 Fluid velocity

The TERI calculated flow velocities were faster near the surface and slower with depth (Table 1A). At approximately 0.7 m depth, velocities were null because no deeper fluid migration was detected in the TERI datasets. This boundary is interpreted as the low permeability soil-bedrock interface at approximately 0.7 m depth which causes soil water to migrate laterally in the downslope direction that the plume was oriented and corresponds to the soil depth determined from excavation. Calculated TERI velocities change by two orders of magnitude across the plot from 12 to 1740 mm/h.

The same approach was taken for transverse Line 3 to make a calculated fluid velocity section from compounded vertical profiles (Table 1B). Results yield the same calculated velocity values for Line 3 at the crossing with Line 1 with a sharp drop to dry vertical profiles at both ends of Line 3 where changes in electrical conductivity did not exceed the background change of 6% increase in conductance.

3.5 Soil moisture data

The soil moisture data indicated a response of sequential vertical wetting at some pits, while others had non sequential wetting with shallower probes remaining dry while deeper probes observed wetting in the subsurface. This was

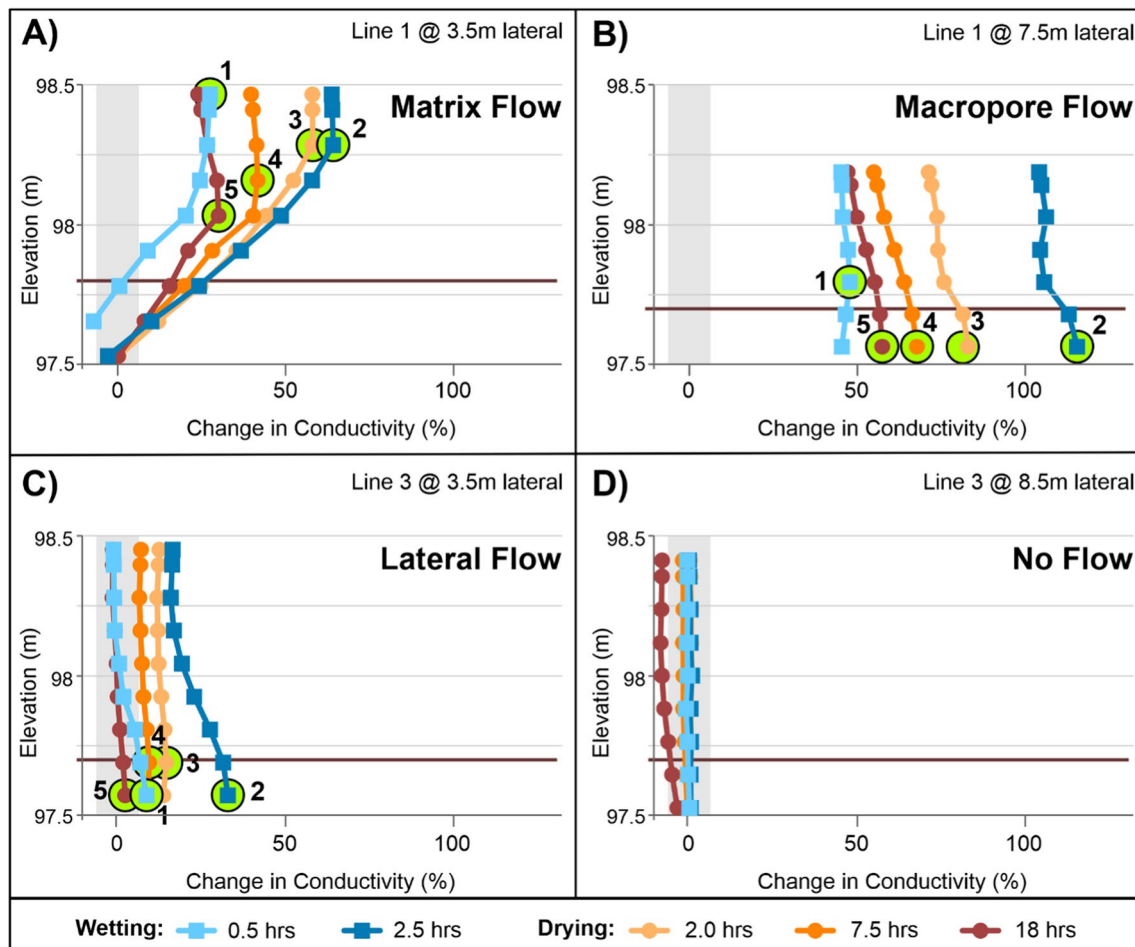


Fig. 9 Summary of four flow patterns of changes in bulk electrical conductivity against elevation observed in TERI datasets above the soil-bedrock interface at 97.5 m elevation. Peak values numbered by time in green circles, noise level indicated in gray shaded area. Horizontal brown line is approximate soil-bedrock interface at 0.7 m depth below land surface in each location. **A** During interpreted matrix flow, the peak values in the data move vertically downward during wetting, points 1 and 2, at a similar rate as during drying. **B** During interpreted macropore flow, during wetting, the data peaks deep in the soil and then at the bedrock contact. During the drying phase, the peak values don't change elevation, just decrease in change of conductance value. **C** Interpreted lateral flow changes occur as weak signature primarily at the soil-bedrock interface outside of the test plot. **D** Interpreted no flow conditions observe no values of bulk electrical conductivity changes outside of the noise level

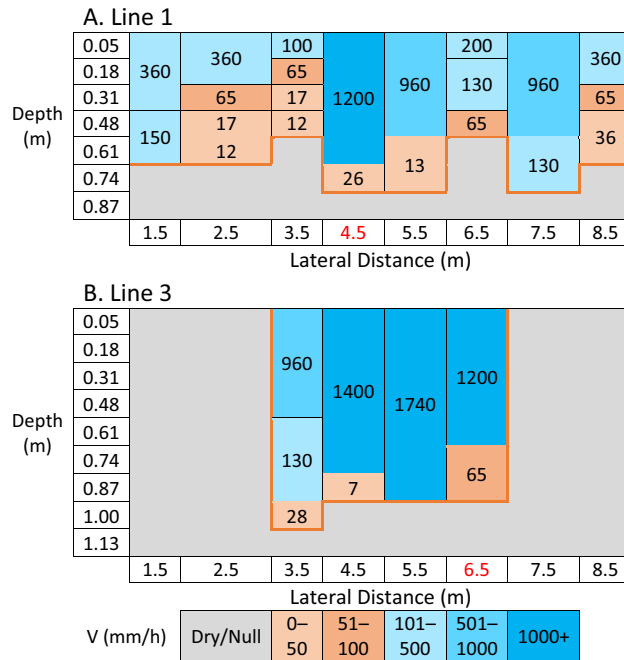
interpreted as the effect of preferential flow. The bedrock interface was approximately 0.7 m deep in the soil pits. Results from another study of the site, Guertault et al. (2021), indicate matrix saturated hydraulic conductivity values between 23 and 36 mm/h [18]. The plot saturated hydraulic conductivity was 44 mm/h, approximately twice the matrix value [18].

4 Discussion

4.1 Can TERI be utilized to calculate wetting front velocities?

The results show wetting of the subsurface that is similar in shape to the distribution expected for both vertical and lateral migration of fluids in soil over bedrock laboratory experiments [23, 24]. Around 0.7 m depth, there is a rapid decrease for changes in bulk electrical conductance (Fig. 4A) and is similar to the location of the significant change in bulk resistivity (Fig. 3A). This depth corresponds to where the competent bedrock limited macropore generation vertically but allowed macropores to develop laterally. The TERI data and subsequent fluid velocity analysis can be compared to what an expected wetting curve should look like along a profile of the line and compared against traditional soil data collected from the adjacent pits. Once calculated velocities have been established using TERI, they can be compared

Table 1 Distribution of calculated macropore velocities based on TERI wetting front velocities in each vertical profile



Results are shown units of in mm/h. Figure 1 shows the location of TERI transects used as data sources. (A) Longitudinal Line 1. The red highlighted cell (4.5 m laterally) represents the location of crossing with transverse Line 3. (B) Transverse Line 3. The red outlined cell (6.5 m laterally) represents the location of crossing with longitudinal Line 1

with velocities obtained using alternative methods to validate the TERI approach. In an experiment at this site, the field plot utilized soil moisture sensors placed below the plot from adjacent soil pits [18]. Results from Guertault et al. [18] in the same field location yield matrix saturated hydraulic conductivity values between 23 and 36 mm/h and plot average hydraulic conductivity of 44 mm/h. The matrix result is similar to values obtained using the TERI approach where the results at the base of the soil at 4.5 and 8.5 m share locations with soil moisture probes for the Guertault et al. [18] experiment (Table 1; Fig. 1). Other locations in the dataset are nearly two orders of magnitude higher and are interpreted as macropore flow influencing fluid velocity and showing more rapid changes with depth and higher magnitude changes in bulk conductivity [18]. The bulk plot hydraulic conductivity value of 44 mm/h would be interpreted as an average of the variability observed by the TERI data. These values may be attributed to a coarse grain matrix, but significant changes were seen in other areas further down the line and near the surface. Coarse grain units were not observed in the soil pits. However, water flow through worm tunnels was observed in the pits during the experiments and macropore flow was also observed out of the profile at the end of the plume, confirming the existence of macropores and flow in them during the experiment (Fig. 2b).

Calculated fluid velocity values in this research have datasets that compare well with the models and data generated from more traditional soil monitoring data sources collected onsite during an adjacent experiment [18]. The change in fluid velocity values within the macropore flow domains are within reason and would support hydraulic conductivity value variations similar to other literature. Mallants et al. [25] studied macropore flow in three types of soil and found hydraulic conductivity values in coarse-grained soil to have a coefficient of variation (CV) of 619%. This would align with the two orders of magnitude difference between macropore flow and matrix flow fluid velocity values in the results for this research. The results suggest that riparian buffers can be designed with these rapid flow paths in mind and if questions about the depth and structure of the macropore network exist, the TERI approach can quantify the structure and the velocity of the macropore network. Permanent cables for TERI monitoring can be installed in critical areas, similar to monitoring wells, to monitor storm events or electrodes can be installed and a cable can be attached for TERI monitoring when needed.

A limiting factor for this method stems from the calculated fluid velocity values. Water can move through the survey area too fast for the instrument to image the wetting front location. In some instances during this experiment, fluid migration reached the interpreted lithological barrier at approximately 0.7 m before the 2.5 h acquisition of all datasets for the time interval was completed. In this case, the area of the vertical profile was saturated to the depth of the interpreted

bedrock boundary in less time than 2.5 h; the highest velocities may not be captured at the site, just a minimum for the fastest values.

The no flow values both laterally and vertically (Figs. 7 and 8) depend on the minimum noise levels that can be obtained with the TERI datasets. If greater levels of noise exist, small signal changes cannot be determined and thus the flow pattern would only distinctly distinguish the highest flow pathways with the strongest signals. By incorporating datasets that go between both saturated and unsaturated surface zone, the noise determination is simpler as locations where no flow exist are more easily evaluated.

4.2 Vertical vs. lateral flow

This analysis focuses on four flow types in which a spatial relationship on the plot can be derived from vertical and lateral flow. Vertical flow was utilized for the fluid velocity calculations (Table 1). During wetting of the plot, areas within the wetting domain had begun to saturate at different rates. TERI data measured the amount of time elapsed for various locations within the wetting domain to infiltrate to an interpreted bedrock boundary, where vertical fluid migration was heavily mitigated. Lateral flow was prevalent outside of the wetting domain on the transverse ERI lines.

These locations also have sporadic vertical fluid migration intervals, different from those seen within the wetting domain. For example, the interpreted lateral flow area (Fig. 7) outside of the wetting domain exhibits peak conductivity values in an order that do not follow the successive increasing changes in saturation patterns observed inside the plot (Figs. 6 and 7). The location of the peaks is different and the pattern is more of a pulse at depth for lateral flow (Fig. 7) compared to an overall vertical increase in vertical macropore flow (Fig. 6). The change between wetting times for peak values are also different orders for the two datasets. This is similar to the pattern in the soil moisture probes where non sequential wetting of the probes would occur with deeper probes getting moisture earlier than shallow probes.

Other techniques can be utilized to extend this type of experiment. GPR has been utilized to observe pumping tests at depth in dolomite [26] but would have difficulty in this setup with obtaining 2D data in a runoff plot unless the antenna setup was built for saturated conditions. Permanent TERI cables can also be installed to allow for observing changes over seasonal variability or to be installed below tilling depth to evaluate an active agricultural field. As acquisition and processing costs decrease, the technique can also be utilized for monitoring over areas of interest for several different applications.

5 Conclusion

The TERI experiment indicates the ability to quantify the movement of water in the subsurface and to calculate the distribution of vertical preferential flow velocity values in a heterogeneous soil using TERI profiles. This information is critical to better characterize hydrologic transport processes in riparian areas and other locations with significant macropore flow. TERI can help accurately locate areas of preferential flow caused by macropores, informing the placement and size of a riparian buffer. Results from this experiment are validated by ordinary soil moisture measurements and literature estimates. The macropore velocity values for macropore flow zones compared to matrix flow zone in this research correspond to a similar ratio of hydraulic conductivity differences with macropore flow in coarse soil [25].

The findings in this research also exhibit definitive lateral and vertical features on the TERI datasets. Lateral features indicate a fluid migration detected outside of the wetting domain in the plot, while vertical features were useful in calculating fluid velocities. Both lateral and vertical TERI features four flow patterns found within the plot during experimentation. The preferential flow velocity calculations varied from 7 mm/h to 1740 mm/h. This significant difference in velocity values over a small area like the test plot supports the delineation of four flow types, matrix flow, macropore flow, lateral flow, and no flow using this method.

Acknowledgements This work was funded by USDA National Institute of Food and Agriculture (NIFA) Project 2016-67019-26855. The work was significantly improved through the work of reviewers for the manuscript and their contributions are highly appreciated. Todd Halihan has a financial interest in Aestus, LLC. An approved management plan is on file in OSU's Office of University Research Compliance.

Author contributions TH and JPH wrote the first draft based on an experiment funded USDA grant written by GAF and TH. TH prepared the manuscript for final publication. LG, JPH, TH, and GAF conducted the field work. BSA assisted with project design and literature comparisons. All authors reviewed the manuscript. All authors read and approved the final manuscript.

Data availability The datasets generated during and/or analyzed during the current study are available from the corresponding author on reasonable request.

Declarations

Competing interests Todd Halihan has a financial interest in Aestus, LLC. An approved management plan is on file in OSU's Office of University Research Compliance.

Open Access This article is licensed under a Creative Commons Attribution 4.0 International License, which permits use, sharing, adaptation, distribution and reproduction in any medium or format, as long as you give appropriate credit to the original author(s) and the source, provide a link to the Creative Commons licence, and indicate if changes were made. The images or other third party material in this article are included in the article's Creative Commons licence, unless indicated otherwise in a credit line to the material. If material is not included in the article's Creative Commons licence and your intended use is not permitted by statutory regulation or exceeds the permitted use, you will need to obtain permission directly from the copyright holder. To view a copy of this licence, visit <http://creativecommons.org/licenses/by/4.0/>.

References

1. Beven K, Germann P. Macropores and water flow in soils. *Water Resour Res.* 1982;18:1311–25. <https://doi.org/10.1029/WR018i005p01311>.
2. Nimmo JR. The processes of preferential flow in the unsaturated zone. *Soil Sci Soc Am J.* 2021;85.1:1–27. <https://doi.org/10.1002/saj.20143>.
3. Jarvis NJ. A review of non-equilibrium water flow and solute transport in soil macropores: principles, controlling factors and consequences for water quality. *Eur J Soil Sci.* 2007;58.3:523–46. <https://doi.org/10.1111/j.1365-2389.2007.00915.x>.
4. Moysey SM, Liu Z. Can the onset of macropore flow be detected using electrical resistivity measurements? *Soil Sci Soc Am J.* 2012;76.1:10–7. <https://doi.org/10.2136/sssaj2010.0413>.
5. Fox GA, Muñoz-Carpena R, Purvis RA. Controlled laboratory experiments and modeling of vegetative filter strips with shallow water tables. *J Hydrol.* 2018;556:1–9. <https://doi.org/10.1016/j.jhydrol.2017.10.069>.
6. Fox GA. Process-based design strengthens the analysis of stream and floodplain systems under a changing climate. *Trans ASABE.* 2019;62.6:1735–42. <https://doi.org/10.13031/trans.13594>.
7. Jarvis N, Koestel J, Larsbo M. Understanding preferential flow in the vadose zone: recent advances and future prospects. *Vadose Zone J.* 2016;15.12:1–11. <https://doi.org/10.2136/vzj2016.09.0075>.
8. Dietrich S, Weinzettel PA, Varni M. Infiltration and drainage analysis in a heterogeneous soil by electrical resistivity tomography. *Soil Sci Soc Am J.* 2014;78.4:1153–67. <https://doi.org/10.2136/sssaj2014.02.0062>.
9. Garré S, Koestel J, Gunther T, Javaux M, Vanderborght J, Vereecken H. Comparison of heterogeneous transport processes observed with electrical resistivity tomography in two soils. *Vadose Zone J.* 2010;9:336–49. <https://doi.org/10.2136/vzj2009.0086>.
10. Halihan T, Hager JP, Guertault L, Fox GA. Detecting macropore fingering using temporal electrical resistivity imaging. *Appl Eng Agric.* 2021;37:861–70. <https://doi.org/10.13031/aea.14294>.
11. Lu D, Zhang C, Sarmah AK, Xia Y, Geng N, Wong JTF, Bundschuh J, Ok YS. *Electrical Resistivity Tomography Monitoring and modeling of preferential flow in Unsaturated Soils.* Soil and Groundwater Rem Technol. CRC Press; 2020. pp. 271–83.
12. Halihan T, Love, Keppel M, Berens V. Analysis of subsurface mound spring connectivity in shale of the western margin of the Great Artesian Basin, South Australia. *Hydrogeol J.* 2013;21:1605–17. <https://doi.org/10.1007/s10040-013-1034-8>.
13. Samouëlian A, Cousin I, Tabbagh A, Bruand A, Richard G. Electrical resistivity survey in soil science: a review. *Soil Tillage Res.* 2005;83:173–93. <https://doi.org/10.1016/j.still.2004.10.004>.
14. Vanella D, Ramírez-Cuesta JM, Sacco A, Longo-Minnolo G, Cirelli GL, Consoli S. Electrical resistivity imaging for monitoring soil water motion patterns under different drip irrigation scenarios. *Irrig Sci.* 2021;39:145–57. <https://doi.org/10.1007/s00271-020-00699-8>.
15. Gao M, Li HY, Liu D, Tang J, Chen X, Chen X, Blöschl G, Leung LR. Identifying the dominant controls on macropore flow velocity in soils: a meta-analysis. *J Hydrol.* 2018;567:590–604. <https://doi.org/10.1016/j.jhydrol.2018.10.044>.
16. Boyles RP, Raman S. Analysis of climate trends in North Carolina (1949–1998). *Environ Int.* 2003;29(2-3):263–75. [https://doi.org/10.1016/S0160-4120\(02\)00185-X](https://doi.org/10.1016/S0160-4120(02)00185-X).
17. Cawthorn JW. *Soil Survey, Wake County, North Carolina, US Soil Conserv Service.* 1970.
18. Guertault L, Fox GA, Halihan T, Muñoz-Carpena R. Quantifying the importance of preferential flow in a riparian buffer. *Trans ASABE.* 2021;64:937–47. <https://doi.org/10.13031/trans.14286>.
19. Halihan T, Paxton S, Graham I, Fenstemaker T, Riley M. Post-remediation evaluation of a LNAPL site using electrical resistivity imaging. *J Environ Monit.* 2005;2005(7):283–7. <https://doi.org/10.1039/B416484A>.
20. Halihan T, Miller RB, Correll D, Heeren DM, Fox GA. Field evidence of a natural capillary barrier in a gravel alluvial aquifer. *Vadose Zone J.* 2019;18.1:1–12. <https://doi.org/10.2136/vzj2018.01.0008>.
21. Miller CR, Routh PS, Brosten TR, McNamara JP. Application of time-lapse ERT imaging to watershed characterization. *Geophysics* 2008; 73.3:1 MJ-Z46. <https://doi.org/10.1190/1.2907156>.
22. Miller RB, Heeren DM, Fox GA, Halihan T, Storm DE, Mittelstet AR. The hydraulic conductivity structure of gravel-dominated vadose zones within alluvial floodplains. *J Hydrol.* 2014;513:229–40. <https://doi.org/10.1016/j.jhydrol.2014.03.046>.
23. Wilson G. Understanding soil-pipe flow and its role in ephemeral gully erosion. *Hydrol Processes.* 2011;25.15:2354–64. <https://doi.org/10.1002/hyp.7998>.
24. Wilson GV, Wells R, Kuhnle R, Fox G, Nieber J. Sediment detachment and transport processes associated with internal erosion of soil pipes. *Earth Surf Processes Landforms.* 2018;43(1):45–63. <https://doi.org/10.1002/esp.4147>.

25. Mallants D, Mohanty BP, Vervoort A, Feyen J. Spatial analysis of saturated hydraulic conductivity in a soil with macropores. *Soil Technol.* 1997;10.2:115 – 31. [https://doi.org/10.1016/S0933-3630\(96\)00093-1](https://doi.org/10.1016/S0933-3630(96)00093-1).
26. Tsoflias GP, Halihan T, Sharp JM. Jr. Monitoring pumping test response in a fractured aquifer using ground-penetrating radar. *Water Resour Res.* 2001;35.5:1221–9. <https://doi.org/10.1029/2000WR900297>.

Publisher's Note Springer Nature remains neutral with regard to jurisdictional claims in published maps and institutional affiliations.